Vol 13 No 2, February 2004
1009-1963/2004/13(02)/0258-06

Chinese Physics

© 2004 Chin. Phys. Soc.
and IOP Publishing Ltd

Optical transitions and upconversion properties of Er^{3+}-doped chloride tellurite glasses *

Wen Lei(温 磊)†, Li Shun-Guang(李顺光), Huang Guo-Song(黄国松), Hu Li-Li(胡丽丽), and Jiang Zhong-Hong(姜中宏)

Shanghai Institute of Optics and Fine Mechanics, Chinese Academy of Sciences, Shanghai 201800, *China*

(Received 28 May 2003; revised manuscript received 23 June 2003)

Er^{3+}-doped lead chloride tellurite glasses were prepared using the conventional melting and quenching method. The absorption spectra were measured and the Judd–Ofelt analysis was performed. The spectroscopic parameters such as the intensity parameters, transition probabilities, radiative lifetimes, and branching ratios were obtained. Intense infrared emission and visible upconversion luminescence under 976 nm excitation were observed. For the 1.55 μm emission, the full width at half maximum and the emission cross sections are more than 50 nm and 8×10^{-20}cm^2, respectively. Three efficient visible luminescences centred at 525, 547, and 658 nm are assigned to the transitions from the excited states $^2H_{11/2}$, $^4S_{3/2}$, and $^4F_{9/2}$ to the ground state $^4I_{15/2}$, respectively. The upconversion mechanisms and the power-dependent intensities are also discussed and evaluated.

Keywords: upconversion material, chloride tellurite glass, spectroscopy, Er^{3+} ion
PACC: 7855, 4255R, 7840

1. Introduction

Rare earth (RE) doped materials have attracted much attention for many years due to their important applications in optical communication systems and upconversion luminescence materials.[1−3] Among these RE ions such as Er^{3+}, Tm^{3+}, Pr^{3+}, and Ho^{3+}, Er^{3+} has been regarded as one of the most efficient for obtaining upconversion emission in visible light regions, as well as the one to be used in optical amplifiers. The 1.55 μm emission band of Er^{3+} is attributed to the $^4I_{13/2} \rightarrow ^4 I_{15/2}$ transition, which corresponds to the third optical communication window and thus can realize signal amplification.[4] In the last decades, upconversion luminescence of RE ions have been investigated extensively owing to their potential applications in visible lasers which are used in the fields of optical storage, color display, undersea transmission, etc.[5−7]

Host material plays an important role in obtaining a strong upconversion signal.[8] Hosts with low phonon energies can reduce the nonradiative loss due to multiphonon relaxation and thus yield a strong upconversion signal.[9] Tellurite glass has low phonon energy (750 cm^{-1}) compared with other oxide glasses and then can decrease the multiphonon loss, which is critical in determining the upconversion efficiency.[10] In parallel, halide glasses have also attracted much attention due to their even lower phonon energies than tellurite glass.[11] However, oxide glasses are more advantageous than other glass systems as host materials for practical use because of high chemical durability and thermal stability. It is expected that mixed glasses including tellurite and halides should bring together the interesting properties of the two systems.[12] To the best knowledge of the present authors, there is still no detailed study on the optical properties of Er^{3+}-doped chloride tellurite glasses.

In this paper, the absorption and emission spectroscopy, lifetime measurements, and the study of infrared to visible upconversion processes of Er^{3+}-doped lead chloride tellurite glasses are investigated. The Judd–Ofelt parameters are deduced from the absorption spectra to obtain theoretical spectroscopic quan-

*Project supported by the Science and Technology Foundation of Shanghai (022261046) and the National Natural Science Foundation of China (60207006).
†E-mail: wenlei@mail.shcnc.ac.cn

tities such as radiative transition probability, branching ratios, and radiative lifetimes. The upconversion luminescence spectra are measured upon excitation at 976 nm light beam. The upconversion mechanisms and power dependent upconversion intensity are discussed and evaluated.

2. Experiments

Er^{3+}-doped glass samples were prepared according to the following compositions TPx in mol%: $(90-x)TeO_2$-$xPbCl_2$-8BaO-$2Yb_2O_3$ (x=0, 5, 10, 15, 20, and 25). All powders are analytically pure with the exception of TeO_2 (99.999%). Er^{3+} doping concentration is 1 mol%, which was introduced as Er_2O_3 with 99.99% purity. About 30 g batches of starting materials were fully mixed and then melted in the corundum crucibles at about 750−800°C in an electronic furnace in non-oxidizing atmosphere for 30 min. The obtained glasses were annealed and cooled to room temperature gradually, and then were cut and polished carefully in order to meet the requirements for optical measurements.

Refractive indices were measured on prism by minimum deviation method. Density measurements were made by Archimedes method with water as the immersion liquid. The absorption spectra were obtained with a Perkin-Elmer-Lambda 900UV/VIS/NIR spectrophotometer from 300 to 1700 nm. We measured the infrared fluorescence spectrum under 976 nm excitation with a TRIAX550 spectrofluorimeter controlled by a computer. The upconversion luminescence spectra in visible light regions were obtained under the same measurement conditions for all samples. A 976 nm laser diode (LD) with a maximum power of 2 W was used as excitation sources. The fluorescence decay of $^4I_{11/2}$ level was measured using a modulated 800 nm laser and a HP546800B 100 MHz oscilloscope. All data were obtained at room temperature.

3. Results and discussion

3.1. Absorption spectra and Judd–Ofelt analysis

The absorption spectra in the visible and near infrared regions of the 1 mol% Er^{3+}-doped TP25 glass is presented in Fig.1. For the material a good transparency is observed in the visible light region extending from 400 nm, indicating the possibility of practical upconversion applications in the visible light region and the negligibility of energy transfer from Er^{3+} to the glass matrix.[13] The spectrum consists of eight absorption peaks at 1530, 976, 799, 653, 544, 522, 489, and 451 nm, corresponding to the transitions from ground state $^4I_{15/2}$ to the excited states $^4I_{13/2}$, $^4I_{11/2}$, $^4I_{9/2}$, $^4F_{9/2}$, $^4S_{3/2}$, $^2H_{11/2}$, $^4F_{7/2}$, and $^4F_{5/2}$, respectively. Judd–Ofelt theory[14,15] is often used to analyse the radiative transition properties. The line strengths, $S_{\rm ed}$, of an electric-dipole absorption transition from the initial state J to the final state J' is given by

$$S_{\rm cal}(J \to J') = S_{\rm ed} = \sum_{t=2,4,6} \Omega_t |< (S,L)J \| U^{(t)} \| (S',L')J' >|, \quad (1)$$

where $\Omega_t S$ (t=2,4,6) are three intensity parameters, and $||U^{(t)}||$ are the double reduced matrix elements of unit tensor operators provided in Ref.[16], which are considered to be independent of the glass matrix.

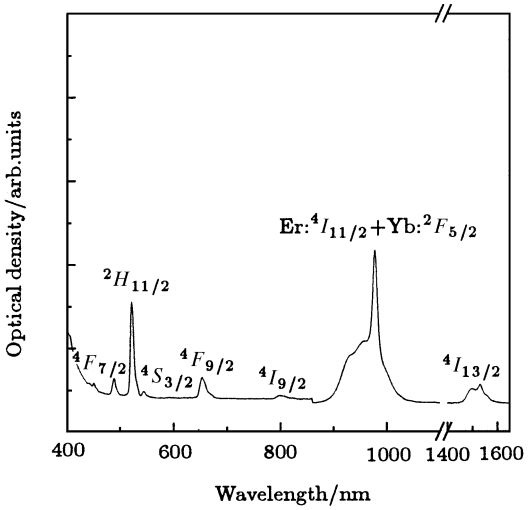


Fig.1. The absorption spectrum of Er^{3+}-doped TP25 glass.

For the transitions between states which meet the rules ΔS=ΔL=0, ΔJ=0, ±1, there exists the contribution of magnetic-dipole transition,

$$S_{\rm md} = \frac{1}{4m^2c^2} |< (S,L)J || L + 2S || (S,L)J >|^2. \quad (2)$$

The measured line strengths, $S_{\rm mea}$ ($J \to J'$), of the emission bands can be determined using the following expression:

$$S_{\rm mea}(J \to J') = \frac{3ch(2J+1)n}{8\pi^3 \lambda e^2 N_0} \times \left[\frac{9}{(n^2+2)^2}\right] \int \alpha(\lambda) {\rm d}\lambda, \quad (3)$$

where J and J' are the total angular momentum quantum numbers of the initial and final states, respec-

tively, n is the refractive index, N_0 is the Er^{3+} concentration, λ is the mean wavelength of the specific absorption band, $\int \alpha(\lambda)\mathrm{d}\lambda$ is the integrated absorption coefficient as a function of λ, and c and h have their usual meaning. The measured line strengths are used to obtain the three parameters Ω_2, Ω_4, and Ω_6 by using at least three absorption bands by a least square method.[17] For the absorption bands, the $^4I_{15/2} \rightarrow ^4 I_{13/2}$ transition contains the contribution of magnetic dipole transition, and the $^4I_{15/2} \rightarrow ^4 I_{11/2}$ transition is influenced largely by the absorption transition $^2F_{7/2} \rightarrow ^2 F_{5/2}$ of Yb^{3+}. Thus, six absorption bands are used to do the least square fit to obtain the three parameters. The measured and calculated line strengths, and the Judd–Ofelt intensity parameters of Er^{3+} in TP25 glass are summarized in Table 1.

Table 1. Measured and calculated absorption line strengths of Er^{3+} in TP25 glass.

Absorption	Energy/cm^{-1}	$S_{\mathrm{mea}}/10^{-20}\,\mathrm{cm}^2$	$S_{\mathrm{cal}}/10^{-20}\,\mathrm{cm}^2$
$^4I_{15/2} \rightarrow ^4 I_{13/2}$	6536	2.649	1.825+0.723 (S_{md})
$^4I_{15/2} \rightarrow ^4 I_{9/2}$	12516	0.279	0.271
$^4I_{15/2} \rightarrow ^4 F_{9/2}$	15314	1.482	1.508
$^4I_{15/2} \rightarrow ^4 S_{3/2}$	18382	0.221	0.235
$^4I_{15/2} \rightarrow ^2 H_{11/2}$	19157	5.104	4.959
$^4I_{15/2} \rightarrow ^4 F_{7/2}$	20450	0.887	0.914
$^4I_{15/2} \rightarrow ^4 F_{5/2}$	22173	0.218	0.230
$\Omega_2 = 5.59 \times 10^{-20}\,\mathrm{cm}^2$, Ω_4=1.82×10^{-20} cm^2, Ω_6=1.03×10^{-20} cm^2			

Parameters Ω_2, Ω_4, and Ω_6 are used to calculate the line strengths corresponding to the transitions from the upper state level to their corresponding low-lying manifold states. Based on these values, the probability of radiative decay between an excited state (J) and the low-lying terminal manifolds (J') is given by

$$\begin{aligned} A(J \rightarrow J') =& A_{\mathrm{ed}} + A_{\mathrm{md}} \\ =& \frac{64\pi^4}{3h\lambda^3(2J+1)} \\ & \times \left[\frac{n(n^2+2)^2}{9} S_{\mathrm{ed}} + n^3 S_{\mathrm{md}}\right], \end{aligned} \quad (4)$$

where A_{ed} and A_{md} are the electric- and magnetic-dipole contributions, respectively.

The radiative lifetime τ_{R} for an excited state (J) is given by

$$\tau_{\mathrm{R}} = 1/\sum A(J \rightarrow J'), \quad (5)$$

where the sum runs over all the final states J'.

The branching ratio, $\beta(J \rightarrow J')$, can be determined from the radiative decay rates by the following expression:

$$\beta(J \rightarrow J') = \frac{A(J \rightarrow J')}{\sum A(J \rightarrow J')} = A(J \rightarrow J')\tau_{\mathrm{R}}. \quad (6)$$

Table 2. Predicted fluorescence line strengths, probability of radiative transition, radiative lifetime, and branching ratios of Er^{3+} in TP25 glass.

Transition	State energy/cm^{-1}	S_{ed}+$S_{\mathrm{md}}/10^{-20}\,\mathrm{cm}^2$	A_{ed}+$A_{\mathrm{md}}/\mathrm{s}^{-1}$	β	τ_{R}/ms
$^4I_{13/2} \rightarrow ^4 I_{15/2}$	6536	1.825+0.723	262.4+99.6	1.0	2.76
$^4I_{11/2} \rightarrow ^4 I_{15/2}$	10235	0.556	358	0.84	2.34
$^4I_{13/2}$	3655	1.389+0.956	42.1+27.8	0.16	
$^4I_{9/2} \rightarrow ^4 I_{15/2}$	12516	0.271	383	0.979	2.56
$^4I_{13/2}$	5980	0.676	2.28	0.006	
$^4I_{11/2}$	2281	0+0.718	5.98	0.015	
$^4F_{9/2} \rightarrow ^4 I_{15/2}$	15314	1.508	3913	0.911	0.23
$^4I_{13/2}$	8778	0.430	210.4	0.049	
$^4I_{11/2}$	5079	1.690	160.9	0.037	
$^4I_{9/2}$	2798	0.560	8.86	0.002	
$^4S_{3/2} \rightarrow ^4 I_{15/2}$	18382	0.235	1758	0.669	0.38
$^4I_{13/2}$	11846	0.358	717.5	0.273	
$^4I_{11/2}$	8147	0.088	57.5	0.022	
$^4I_{9/2}$	3068	0.396	96.3	0.037	

Table 2 presents the calculated results of radiative transition probability, radiative lifetimes, and branching ratios in Er^{3+}-doped TP25 glass. The radiative transition probability for $^4I_{13/2}$ level is $362\,s^{-1}$, which is much higher than those in silicate, phosphate, and germanate glasses. The branching ratio is a critical parameter for the laser designer, resulting from its characterization on the possibility of attaining stimulated emission from any specific transition. The branching ratios for the transitions $^4S_{3/2} \rightarrow ^4 I_{15/2}$ and $^4F_{9/2} \rightarrow ^4 I_{15/2}$ are 67% and 91%, respectively. Therefore, it is possible to obtain efficient green and red emissions in the glasses under 976 nm excitation.

3.2. Infrared and upconversion fluorescences

Figure 2 illustrates the fluorescence spectrum of Er^{3+}-doped TP25 glass. The full width at half maximum (FWHM) is often used to evaluate the bandwidth of the spectrum, and the FWHM value in Fig.2 is 56 nm. The peak wavelength for the emission is 1533 nm. The absorption cross sections were determined from the measured absorption spectrum, and the emission cross sections were calculated from the absorption cross sections by the McCumber theory.[18] The peak values of absorption cross section and emission cross section are $7.6\times10^{-21}\,cm^2$ and $8.3\times10^{-21}\,cm^2$, respectively.

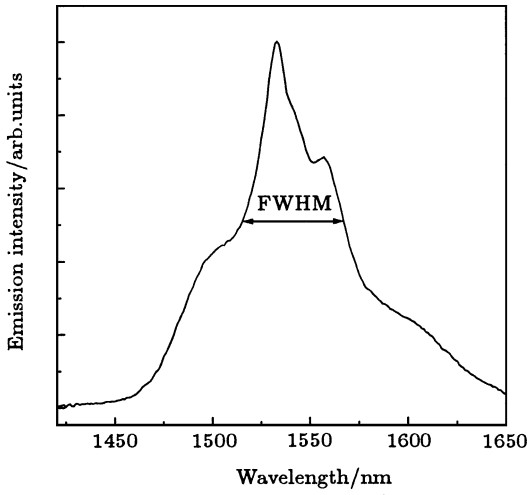


Fig.2. Infrared fluorescence spectrum of Er^{3+}-doped TP25 glass.

Figure 3 shows the upconversion spectra of Er^{3+} in TZL, TPx15, and TPx25 glasses. Three emission bands centred at 525, 547, and 657 nm, which correspond to the transitions $^2H_{11/2} \rightarrow ^4 I_{15/2}$, $^4S_{3/2} \rightarrow ^4I_{15/2}$, and $^4F_{9/2} \rightarrow ^4I_{15/2}$, respectively, are simultaneously observed. It can be seen that all the emission intensities in the glasses containing chloride ions are much stronger than the TZL glass without chloride ion. This fact confirms the expectation that chloride ions with low phonon energy contribute much to the increase of upconversion intensity at room temperature. For the glass samples with $PbCl_2$ content more than 20 mol%, the green emission is bright enough to be observed by the naked eye at an excitation power as low as 60 mW. Figure 4 illustrates the dependence of upconversion intensity on the $PbCl_2$ content in the glass. The intensity of green emission at 525 nm almost does not change with increasing $PbCl_2$ content, while the emission intensities at 547 and 657 nm increase slightly in the range of 10–20 mol% of $PbCl_2$ content and then increase markedly as $PbCl_2$ increases. Furthermore, the red emission intensity enhances much larger than the green emission intensity. These results suggest that $PbCl_2$ has more influence on the red emission than on the green emissions.

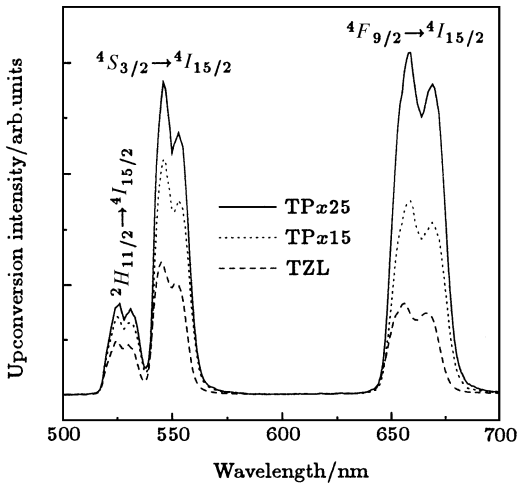


Fig.3. Upconversion spectra of Er^{3+}/Yb^{3+}-doped TZL, TPCB10, and TPCB20 glasses upon excitation at 976 nm.

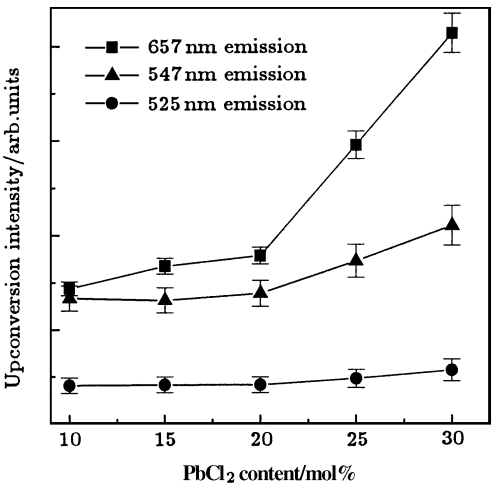


Fig.4. Dependence of upconversion intensities on $PbCl_2$ content in Er^{3+}-doped lead chloride tellurite glasses.

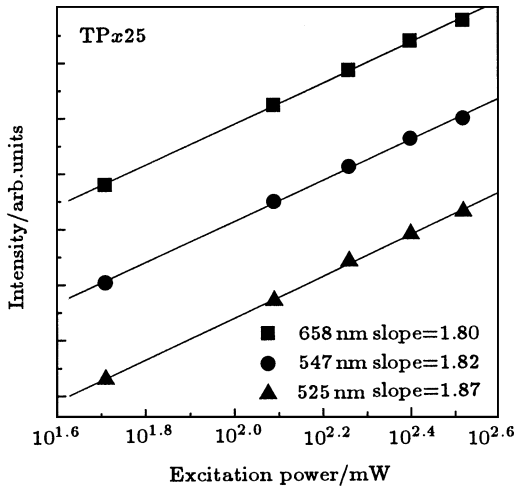


Fig.5. Dependence of the emission intensities on 976 nm excitation power of Er^{3+} in TPx25 glass.

The number of absorbed photons for the upconversion emissions was determined by plotting the upconversion intensity as a function of the pumping power, as shown in Fig.5. The results indicate that two photon steps are involved in the upconversion processes. According to the energy matching conditions and the quadratic dependence on excitation power, the possible upconversion mechanisms are discussed and indicated in the simplified energy levels of Er^{3+}, as illustrated in Fig.6.[19−21] For the green emissions, in the first step, the $^4I_{11/2}$ level is directly excited by energy transfer (ET) processes from Yb^{3+} to Er^{3+}, where Yb^{3+} absorbs the excitation photon directly, inducing the $^2F_{7/2} \rightarrow {}^2F_{5/2}$ transition. Since the absorption cross section of Yb^{3+} in the excitation wavelength region is much larger than that of Er^{3+}, the ET process from Yb^{3+} to Er^{3+} mainly contributes to the first step. The measured lifetime of $^4I_{11/2}$ level of Er^{3+} in the samples are about 400 μs, which is longer than that in tellurite glass (200 μs) and much longer than those in other conventional glass hosts.[21] The long-lived $^4I_{11/2}$ level as an intermediate state then undoubtedly stimulates other energy transfer processes. As a result, the second step involves the excitation of Er^{3+} in $^4I_{11/2}$ level to $^4F_{7/2}$ level by means of cross relaxation (CR), $^4I_{11/2} + {}^4I_{11/2} \rightarrow {}^4F_{7/2} + {}^4I_{15/2}$, and/or excited state absorption (ESA), $^4I_{11/2}$+a photon $\rightarrow {}^4F_{7/2}$, and/or by ET from Yb^{3+} to Er^{3+}, $^2F_{5/2}$ (Yb^{3+}) + $^4I_{11/2}$ (Er^{3+}) $\rightarrow {}^2F_{7/2}$ (Yb^{3+}) + $^4F_{7/2}$ (Er^{3+}), processes. The populated Er^{3+} $^4F_{7/2}$ level then relaxes rapidly and nonradiatively to the next lower levels $^2H_{11/2}$ and $^4S_{3/2}$, resulting from the small energy gap between them. The $^2H_{11/2} \rightarrow {}^4I_{15/2}$ emission is observed whenever the $^4S_{3/2}$ level is excited owing to a fast equilibrium between these two levels 26 and 27. Besides, for the red upconversion around 655 nm, the population of $^4F_{9/2}$ level is ascribed to the combined results of ET processes based on $^4I_{13/2}$ level which is populated by multiphonon relaxation process from $^4I_{11/2}$ level: ESA ($^4I_{13/2}$+a photon $\rightarrow {}^4F_{9/2}$), CR between Er^{3+} ions: $^4I_{13/2} + {}^4I_{11/2} \rightarrow {}^4I_{15/2} + {}^4F_{9/2}$, and ET from Yb^{3+} to Er^{3+} (Yb^{3+}: $^2F_{5/2}$+Er^{3+}: $^4I_{13/2} \rightarrow Yb^{3+}$: $^2F_{7/2}$+Er^{3+}: $^4F_{9/2}$), and a contribution of nonradiative relaxation from higher energy level $^4S_{3/2}$ populated by means of the process described previously.

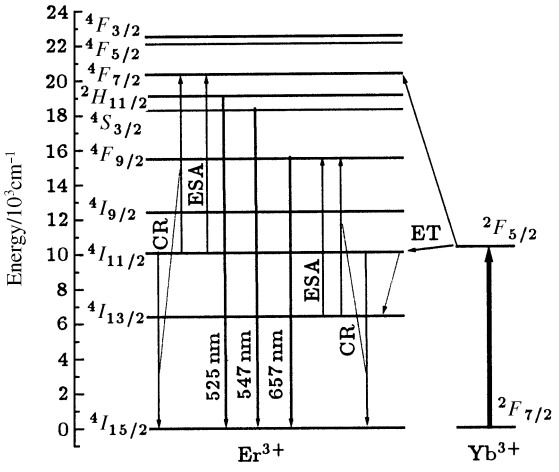


Fig.6. Simplified energy level diagram of Er^{3+} and Yb^{3+} and possible transition pathways in Er^{3+}/Yb^{3+}-doped lead chloride tellurite glasses.

4. Conclusion

We have calculated the spectroscopic parameters such as intensity parameters, the radiative transition probabilities, the branching ratios, and the radiative lifetimes of Er^{3+}-doped lead chloride tellurite glasses. Intense infrared emission and upconversion luminescence spectra under 976 nm excitation are obtained. For the infrared emission, the FWHMs and the emission cross sections are more than 50 nm and 8×10^{-20} cm^2, respectively. Three efficient visible emissions centred at 525, 547, and 658 nm are observed and are assigned to the transitions from $^2H_{11/2}$, $^4S_{3/2}$, and $^4F_{9/2}$ to the ground state $^4I_{15/2}$, respectively. The three upconversion luminescences are due to two-photon processes and the upconversion intensities are influenced by the content of $PbCl_2$ in the glass. The results obtained might provide valuable information in developing optical amplifiers and visi-

ble upconversion lasers which are used in the fields of colour display, optical data storage, undersea transmission, etc.

Acknowledgement

The authors would like to thank Dr. Yang Jian-Hu for helpful discussions.

References

[1] Liang J J 2000 *Chin. Phys.* **9** 783
[2] Chen X B, Deng Z W, Meng C, Zhang G Y and Li M X 2000 *Chin. Phys.* **9** 379
[3] Yang J H, Dai S X, Zhou Y F, Wen L, Hu L L and Jiang Z H 2003 *J. Appl. Phys.* **93** 977
[4] Yang J H, Dai S X, Wen L, Liu Z P, Hu L L and Jiang Z H 2003 *Acta Phys. Sin.* **52** 508 (in Chinese)
[5] Poirier G, Jerez V A, Araújo C B, Messaddeq Y, Ribeiro S J L and Poulain M 2003 *J. Appl. Phys.* **93** 1493
[6] Dai S X, Yang J H, Liu Z P, Wen L, Hu L L and Jiang Z H 2003 *Acta Phys. Sin.* **52** 729 (in Chinese)
[7] Wang Y and Ohwaki J 1993 *J. Appl. Phys.* **74** 1272
[8] Hirao K, Kishimoto S, Tanaka K, Tanabe S and Soga N 1992 *J. Non-Cryst. Solids* **139** 151
[9] Tanabe S, Yoshii S, Hirao K and Soga N 1992 *Phys. Rev.* B **45** 4620
[10] Vetrone F, Boyer J C, Capobianco J A, Speghini A and Bettinelli M 2002 *Appl. Phys. Lett.* **80** 1752
[11] Güdel H U and Pollnau M 2000 *J. Alloys Comp.* **303-304** 307
[12] Silva M A P, Messaddeq Y, Briois V, Poulain M, Villain F and Riberiro S J L 2002 *J. Phys. Chem. Solids* **63** 605
[13] Ivanova T Y, Man'shina A A, Kurochkin A V, Tver'yanovich Y S and Smirnov V B 2002 *J. Non-Cryst. Solids* **298** 7
[14] Judd B R 1962 *Phys. Rev.* **127** 750
[15] Ofelt G S 1962 *J. Chem. Phys.* **37** 511
[16] Carnall W T, Fields P R and Wybourne B G 1965 *J. Chem. Phys.* **42** 3797
[17] Yang J H, Dai S X, Hu L L, Jiang Z H and Li S G 2003 *Acta Opt. Sin.* **22** 210 (in Chinese)
[18] McCumber D E 1964 *Phys. Rev.* A **134** 299
[19] Auzel F 1990 *J. Lumin.* **45** 341
[20] Joubert M F 1999 *Opt. Mater.* **11** 181
[21] Choi Y G, Lim D S, Kim K H, Cho D H and Lee H K 1999 *Electron. Lett.* **35** 1765